Simulation of Wind Field in a Building Complex for Evaluation of the Wind Effect Along UAS Flight Path

Joshua Christian Nathanael* and C. H. John Wang†
Air Traffic Management Research Institute (ATMRI), Nanyang Technological University
65 Nanyang Drive, Singapore 637460

Kin Huat Low‡
School of Mechanical and Aerospace Engineering, Nanyang Technological University
50 Nanyang Avenue, Singapore 639798

With the use of Unmanned Aerial Systems (UAS) becoming more common, wind field within urban environments becomes significant, and its impact on UAS flight should be examined to ensure UAS operations can be implemented and managed safely with little to no risk of damages and injuries to the inhabitants and infrastructures. This study presents the wind field within the Biopolis building complex in Singapore from steady-state RANS simulation using OpenFOAM v1912. The wind simulation was done using various inlet wind speeds and directions based on the measurements from a weather station near the building complex. After obtaining the velocity field for the whole area, the wind effect on UAS along a given flight path was inferred from the local wind velocity magnitude and direction along the path. When the general wind heading was aligned with the flight path, the local wind and its impact on the UAS along its path had more gradual and less extreme changes than in other cases where the UAS had to fly by crossing through the wake flow of the buildings. Additionally, for flow cases with the same inlet wind direction but different reference speeds, similarity in their results was observed when the wind velocity magnitude was normalized with respect to the velocity magnitude at the inlet boundary. Contours of the wind Turbulence Kinetic Energy (TKE) from the simulation results show that the areas with higher TKE are located around buildings at the most upstream against the wind, and these areas increase in size and TKE levels with higher wind speed.

I. Introduction

Computational Fluid Dynamics (CFD) is a useful analysis tool to study the dynamics and patterns of fluids in a given set of boundary conditions. It has been utilized to study a wide range of flow cases, including to study the wind field around a building or within a complex of several buildings. CFD simulations have been employed to study the wind loading on a single building [1–3], as well as the pressure and speed of the air around the building [3, 4]. Furthermore, increasing number of studies have incorporated an urban environment consisting of multiple buildings into wind field simulation [5–9], the results of which have been validated with field measurements to ensure their accuracy. Results from the wind field simulation may vary depending on the simulation setup, such as the amount of buildings that are included and the details of the environment surrounding the area of interest [6–8], and also the wind direction from the velocity inlet [9].

Meanwhile, with the use of Unmanned Aerial Systems (UAS) becoming more prevalent around the world, wind field within urban environments becomes more significant and several studies have examined its impact on UAS flight performance. Sutherland et al. [10] studied the UAS flight controller ability to maintain the UAS within its assigned position or path amidst transient wind flow. From the obtained time-averaged solution of CFD simulation [11], Watkins et al. [12] focused on the change in flow velocity magnitude and angles due to the shear flow over a building's roof. Murray and Anderson [13] showed that the stability of UAS is dependent on the Turbulence Kinetic Energy of the wind field, and therefore UAS operations should be mindful of their operating conditions such as the altitude, wind speed and direction. To allow further adoption of UAS technology within urban environments, the safety of all inhabitants and infrastructures within them has to be guaranteed first to prevent any casualties due to UAS accidents.

*Project Officer, Unmanned Aerial Systems (UAS) Programme, ATMRI, NTU
†Senior Research Fellow, Assistant Programme Director, UAS Programme, ATMRI, NTU
‡Professor, School of Mechanical and Aerospace Engineering; Corresponding author, e-mail: mkhlow@ntu.edu.sg

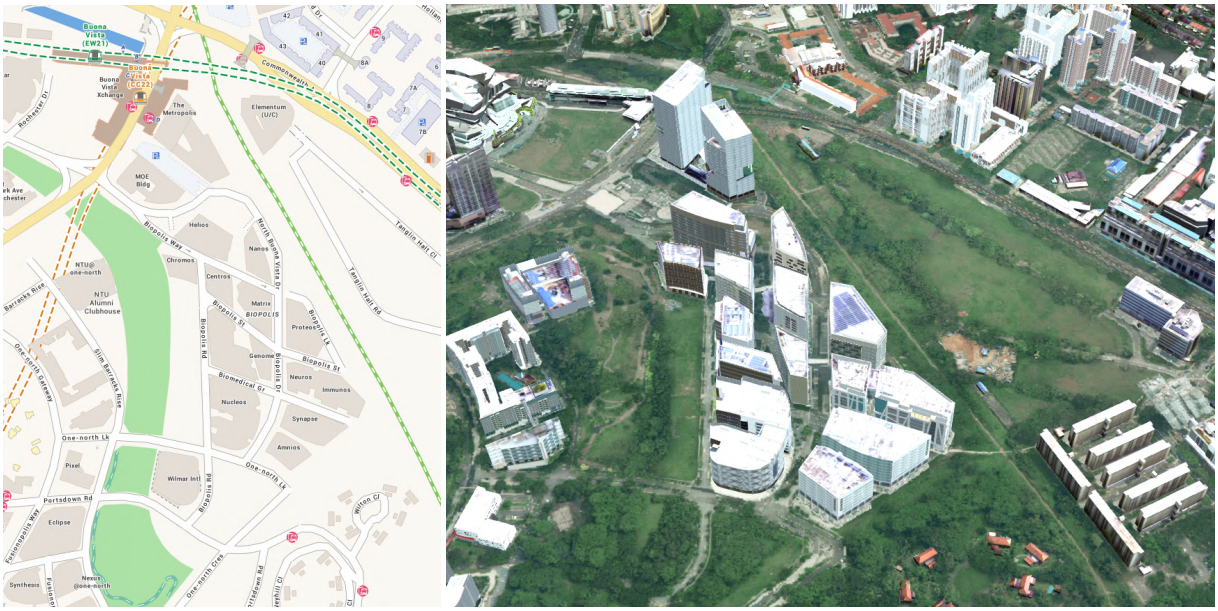

(a) 2D layout **(b) 3D render**

Fig. 1 Map of the Biopolis building complex in 2D and the 3D render from OneMap3D website.

This paper presents the flow simulation results of the wind field in the Biopolis building complex in the One-North area in Singapore (Figure 1), as part of assessing the safety and feasibility of implementing UAS operations within the area. Following this introduction, Section II shows the trend in wind speed and direction throughout a year as obtained from the Realtime Weather Readings across Singapore, managed by the National Environment Agency (NEA) and made available on the Data.gov.sg website [14] under the terms of the Singapore Open Data Licence version 1.0 [15]. After narrowing down and deciding the dominant range of speed and direction, the wind condition was incorporated into the wind field simulation setup in OpenFOAM v1912 as detailed in Section III. Following that, Section IV presents the wind field in the Biopolis complex for various inlet wind speeds and directions, and the difference in inflow of air experienced by UAS when flying through different paths. Finally, Section V summarizes what has been presented in this paper, along with the future work to improve current method and results, and apply them for managing UAS operations.

II. Analysis of Weather Readings

Before beginning the wind field simulation, the wind condition within the area of interest should be identified beforehand as it will determine the inlet boundary condition required for the flow simulation. Although ideally there should have been wind measurements in the Biopolis building complex prior to simulating the wind field in the area, for this study the wind condition was approximated with measurements from nearby weather stations, which are operated by the Meteorological Service Singapore (MSS), a division under the NEA. Figure 2 shows the map of Singapore, with markings showing the location of the Biopolis complex and weather stations across the island. Most Automatic Weather Stations only record the amount of rainfall in their respective area, and only a few are also equipped to measure wind speed and direction. This narrowed down the list of weather stations that could be chosen for this study, and the two possible weather stations that are the closest to Biopolis are S50 in Clementi and S116 in Pasir Panjang. The surroundings at the two weather stations are shown in Figure 3.

The wind measurements provided on Data.gov.sg can be accessed after entering the date and time input. If the date alone is entered, the data will include all measurements recorded on the given date. The output data includes all other weather stations in addition to S50 and S116, and observing the trend in wind data for an entire year requires repeated input of different dates to generate all the necessary data. Therefore, a Python script was created to automate the task of filtering and compiling the wind data from Data.gov.sg, then the desired wind data output for each month could be processed further and turned into wind roses. With these wind roses, trend in the wind conditions for every month of the year could be visualized to determine the dominant range of wind speeds and directions in the chosen area.

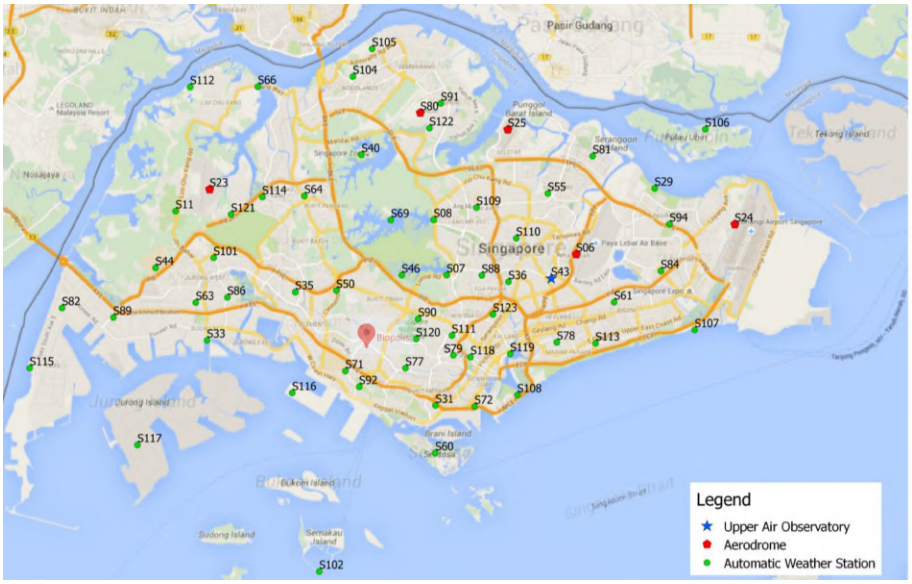

Fig. 2 Map of Singapore showing the locations of weather stations [16] and the Biopolis complex.

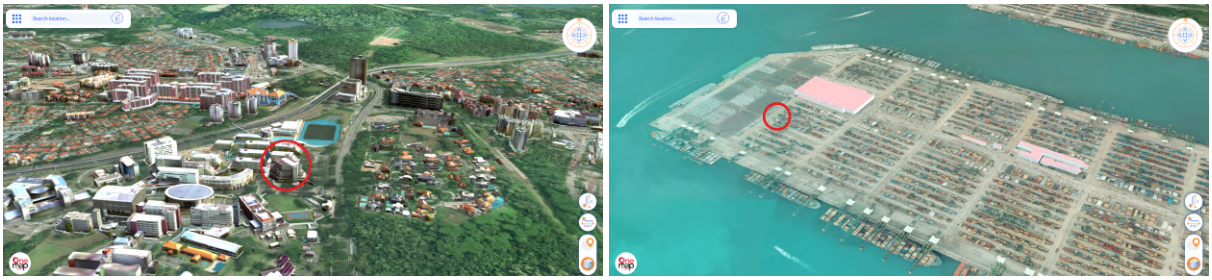

(a) S50 Clementi **(b) S116 Pasir Panjang**

Fig. 3 3D renders (from OneMap3D website) of the buildings at S50 Clementi and S116 Pasir Panjang, with red circles marking the locations of the weather stations.

Figure 4 shows the wind roses for the wind field at S50 Clementi and S116 Pasir Panjang weather stations in July and December 2021. The wind roses show the distribution of wind direction and speed that occurred in the specified location. The angles shown outside of the circle in the diagrams indicate the direction from which the wind was coming, while the percentage indicates the frequency of the wind coming from the given direction. Wind rose with a more pointed shape and higher percentage shows that the wind generally comes from the same direction, while wind rose with a more spread out shape and lower percentage means the wind direction tends to vary. Additionally, the various colors shown in the wind roses indicate the different ranges of wind speed that occurred, and the thickness of each color indicates the frequency of the wind blowing within each speed range.

At both weather stations, the dominant wind direction in July is Southeasterly to Southerly, while in December it is Northerly to Northeasterly. This is in accordance to the general prevailing wind directions due to two main seasons in Singapore, the Southwest Monsoon Season and the Northeast Monsoon Season respectively [17]. At S116 Pasir Panjang the wind speed was usually in the 6 - 9 knots (3.1 - 4.6 m/s) range in July and December 2021 with strong gusts also recorded albeit infrequent, while at S50 Clementi the wind speed in the 3 - 6 knots (1.5 - 3.1 m/s) range was more common. The higher wind speed at S116 Pasir Panjang than at S50 Clementi is likely due to the difference in terrain and surroundings of the two weather stations. The S116 Pasir Panjang station is located near the sea with light weight low rise constructions, while the S50 Clementi station is within an environment with compact mid rise buildings [18]. The Biopolis building complex is situated in a developed environment with numerous buildings, thus making it more similar to the S50 Clementi station than S116 Pasir Panjang. Therefore, the inlet wind speed and direction for simulating the wind field in Biopolis would use the wind measurements from the S50 Clementi weather station.

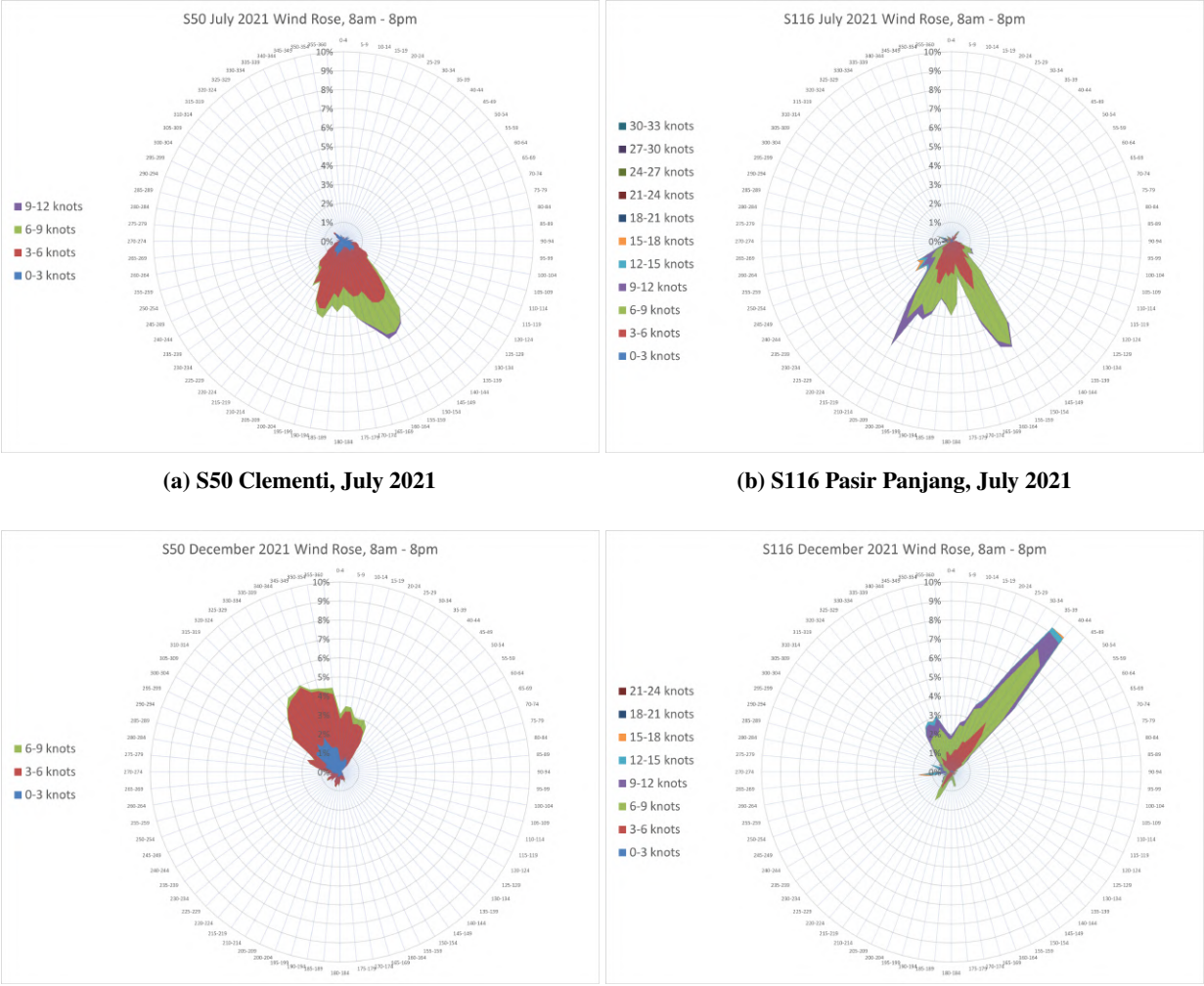

(a) S50 Clementi, July 2021 **(b) S116 Pasir Panjang, July 2021**

(c) S50 Clementi, December 2021 **(d) S116 Pasir Panjang, December 2021**

Fig. 4 Wind roses based on wind measurements at S50 and S116 weather stations in July and December 2021.

III. Wind Field Simulation Setup

A. Meshing in OpenFOAM v1912

Simulation of wind field in Biopolis for this study used the open-source CFD software OpenFOAM v1912. Firstly, 3D CAD geometry of the buildings and terrain in Biopolis were prepared. Figure 5 shows the three CAD geometry files that were included for the meshing process in OpenFOAM. The models and coordinates of the buildings (the grey-colored blocks) were provided by the Housing Development Board (HDB) and Singapore Land Authority (SLA) in 2016, while the terrain (the green-colored base) was processed from the ground elevation model based on the data acquired during the Shuttle Radar Topography Mission (SRTM) by National Aeronautics and Space Administration (NASA) and National Geospatial-Intelligence Agency (NGA) in 2000 [19]. The edges of elevation model for the detailed terrain were smoothed down to transition into a flat surface (the brown-colored plain) which was for the inflow development of the boundary layer. The geometry files were separated instead of combined into one whole, so that different settings of mesh resolution and surface roughness could be assigned to the surface of each part later on.

To create the mesh for wind field simulation in OpenFOAM, several utilities that are available from the software were used. First, the utility blockMesh was used to create a rectangle block of mesh with uniform resolution of 20 meters. The coordinates and dimensions of the block, number of cell divisions along its three axes, as well as the sides that would become the inlet, outlet, symmetry, and non-slip ground were specified in the settings found in the file

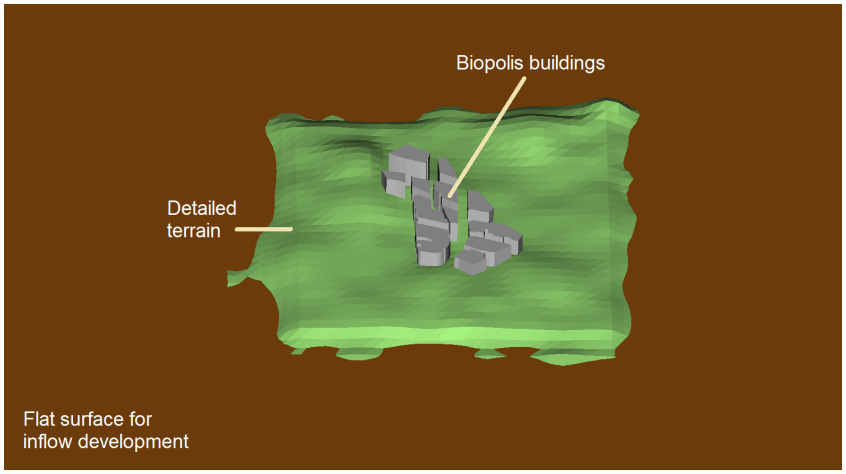

Fig. 5 3D CAD geometry of the terrain and buildings in Biopolis for wind field simulation.

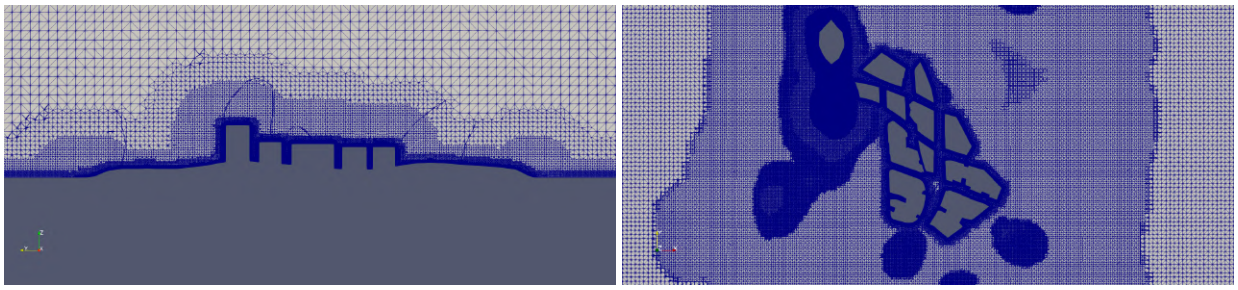

(a) Vertical plane **(b) Horizontal plane**

Fig. 6 Views of the mesh created with snappyHexMesh utility in OpenFOAM on vertical and horizontal plane.

blockMeshDict. The length, width and height of the mesh block was 3.08 x 3.08 x 0.9 km. The lateral and top sides of the block mesh were at a distance of around $12H$ and $8H$ from the outer edge of the building blocks respectively, where H is the highest Z-coordinate in the buildings CAD geometry file, to minimize the effect of wake flow from the buildings on the block mesh boundaries [9, 20].

The inlet and outlet of the block mesh were initially set such that the wind would be blowing from west to east. When simulating the wind field with different wind directions, the utility rotateMesh was used for every case by entering the initial and final direction the outlet was facing, so that the block mesh could be rotated to fit the wind direction that would be set. After it was rotated, the block mesh was fitted and refined around the buildings and terrain geometry using the snappyHexMesh utility. Applying rotateMesh before snappyHexMesh allowed the mesh to be rotated following the desired wind direction, while still maintaining the position and orientation of the buildings and terrain geometry. In the settings file of snappyHexMeshDict, the different levels of mesh refinement, the distance from surfaces in which each level was applicable, and the minimum of 5 cells between successive levels were specified. With this, mesh resolution of 2.5 m on the flat surface and 1.25 m on the buildings and detailed terrain could be achieved. Figure 6 shows the resulting mesh with different levels of refinement as viewed from a vertical and horizontal slicing plane.

B. Setup for Boundary Conditions

In OpenFOAM v1912, tutorial examples for various flow cases are available and the tutorial windAroundBuildings was used as a basis for setting up the wind simulation in this study. The boundary conditions and settings discussed in this section are the changes that were made to the original settings provided in the tutorial case. After the mesh was created, the values of various variables needed to be initialized for the mesh boundaries. The variables are velocity (U), static pressure (p), turbulence kinetic energy (k), turbulence dissipation rate (ϵ), and turbulence viscosity (ν_t). For every variable there was a file that indicated the initial value at the following mesh boundaries: inlet, outlet, symmetry,

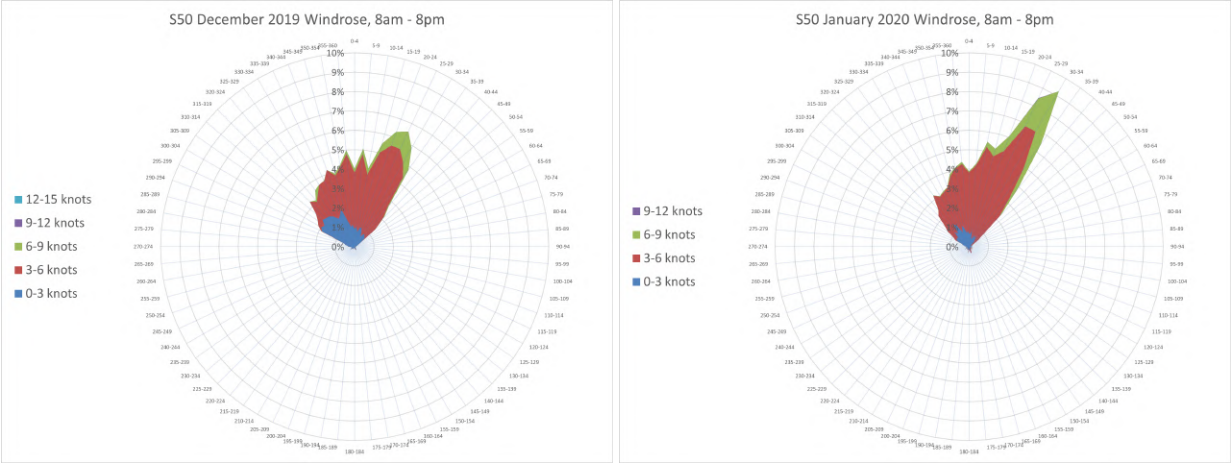

(a) S50 Clementi, December 2019 **(b) S50 Clementi, January 2020**

Fig. 7 Wind roses based on wind measurements at S50 weather station in December 2019 and January 2020.

and the non-slip surfaces consisting of the buildings, middle terrain, and distant plain. At the inlet and outlet, the atmBoundaryLayer base class was used to assign the Atmospheric Boundary Layer (ABL) profile for U, k, and ϵ with reference height (z_{ref}) of 10 meters and aerodynamic roughness length (z_0) of 1 meter. The atmBoundaryLayer class assigns the incoming flow with the specified ABL profile at the inlet, and applies zero-gradient approximation for outgoing flow at the outlet, so this allowed the same boundary conditions to be given for both the inlet and outlet.

The reference speed (U_{ref}) and flow direction could be specified in the atmBoundaryLayer settings according to the speeds and directions of the wind that would be simulated. To narrow the range of wind conditions for the simulation in this study, the chosen values would follow the speed and direction during the Northeast Monsoon Season in December and January. In December 2021 (Figure 4c), it appears that it was more common for the wind at S50 Clementi to be northwesterly (coming from 320 - 360 degrees), while in December 2019 and January 2020 (Figure 7) a northeasterly wind (coming from 015 - 040 degrees) appears to be more common. In any case, the wind speed was usually within the 0 - 9 knots (0 - 4.6 m/s) range with 3 - 6 knots (1.5 - 3.1 m/s) being the most common range. Hence, the simulation of wind field in Biopolis covered the range of 1 - 4 m/s for the wind speed and 320 to 040 degrees for the wind direction.

For p, the inlet values used zero-gradient approximation and the outlet values were fixed at zero static pressure. For ν_t, the effect of surface roughness was added onto the middle terrain and distant plain by using the nutkRoughWallFunction type and specifying the roughness height (k_s) and roughness constant (C_s) [6, 7, 9]. The roughness length z_0 could expressed in terms of k_s and C_s using the relationship $k_s C_s = 9.793 z_0$ proposed by Blocken, et al. [21]. Following the setup by Wise, et al. [9], the z_0 for the middle terrain was 0.1 m to account for the effects from trees, lighting poles and other features, and the z_0 for the distant plain was 1 m to represent the surrounding buildings not included in the simulation. The value k_s should be smaller than the height of cell center near the terrain surface. Since the mesh resolution was 1.25 m on the middle terrain and 2.5 m on the distant plain, the value of k_s for the middle terrain and distant plain was set to 0.6 and 1.2 meters respectively, and then the value for C_s could be calculated for each surface.

C. Numerical Solver and Schemes

As this wind field study is currently in the preliminary phase to discover the velocity field within a building complex, the steady-state incompressible solver simpleFoam in OpenFOAM v1912 was used with the Reynolds-Averaged Navier Stokes (RANS) turbulence model for numerous flow cases using different wind speeds and directions. Using steady-state solver with RANS turbulence model is less computationally expensive compared to transient flow simulations using other approaches of turbulence modeling such as the Large Eddy Simulation (LES) or Detached Eddy Simulation (DES). The simpleFoam solver uses the SIMPLE (Semi-Implicit Method for Pressure Linked Equations) algorithm to iteratively solve the flow equations. The Realizable k-ϵ model was applied for solving the wind turbulence properties. The discretization scheme for the gradient terms of variables U, k and ϵ used the cellLimited version of the leastSquares method. For the convective divergence terms of U, k and ϵ, the scheme used was the bounded form of the Gaussian integration method with linearUpwind interpolation scheme using the aforementioned gradient scheme.

IV. Results

A. Mesh Convergence Study

Before running wind simulation using various wind speeds and directions, mesh convergence study was carried out to ensure the refinement applied for the mesh was sufficient such that the obtained results were independent of the mesh and applied refinement. To do this, meshes with differing number of cells were created by applying different levels of refinement during the meshing process. In the settings file snappyHexMeshDict, the different levels of mesh refinement could be specified together with the distance from surfaces in which each level was applied. Higher level of refinement could be specified for the cells nearer to the surfaces, and the distance from surfaces could be reduced for coarser mesh or extended for finer mesh. In this manner, four different meshes were created: a coarse mesh with 17.3 million cells, a baseline mesh with 17.6 million cells, a fine mesh with 18.1 million cells, and the finest mesh with 23.2 million cells.

The setup for each mesh used the same wind condition with reference speed 2 m/s and direction 000 degrees (from the north). From the simulation results, velocity magnitude contours were produced, and velocity magnitude plots were created using the data extracted along two path lines. Path 1 was chosen along a street more upstream to the incoming wind, while Path 2 went through a street further downstream on the south side. Figure 8 shows the wind velocity magnitude contours and plots of local wind speed along the two paths indicated by the arrows displayed on the contours. Figure 8a shows the velocity magnitude along a vertical path and its increase from Z = 100 meters upwards due to the flow shearing caused by the taller northernmost building. The horizontal plane shown in Figure 8b was taken at Z = 50 meters, where the plane sliced through all buildings in the complex, to show the regions with high and low local velocity magnitude as the wind goes around the buildings through the passages in between. Buildings in this figure were labelled with letters to clarify the positions along the horizontal paths where the velocity magnitude rose and fell.

The profiles of local wind velocity magnitude along the vertical path shown in Figure 8a shows that the results from different meshes matched closely, and the profiles along horizontal paths shown in Figure 8b were also in general agreement with little difference at some places. Along horizontal paths, the results from different meshes agreed more closely when the wind was not affected by the buildings. The velocity profiles became slightly varied when the position was in between or behind buildings where the velocity magnitude was lower, such as behind Buildings A and B on Path 1 and Buildings D and E on Path 2. The peaks in the velocity profiles also differed between the meshes such as when the position was before Building B on Path 1 and before and after Building E on Path 2. While there were some discrepancies, they were small enough that the baseline mesh was deemed to be sufficient in capturing the general flow details of the wind field within the Biopolis building complex. The levels of refinement in the meshing settings for creating the baseline mesh would therefore be also used in the other cases using different wind speeds and directions.

B. Velocity Field from Different Inlet Wind Directions

Simulation of wind field in Biopolis was done for various wind speeds (1 - 4 m/s) and directions (coming from 320 to 040 degrees). In this section, the wind velocity field results were obtained from simulation using different wind directions, but with the same reference speed of 2 m/s. While the wind simulation were carried out with smaller intervals between different wind directions, for the sake of brevity and clarity only three sets of results are presented here: northwesterly wind from 320 degrees, northerly wind from 000 degrees, and northeasterly wind from 040 degrees. Figure 9 shows the wind velocity magnitude contours on a horizontal plane from simulation using wind directions from 320, 000, and 040 degrees. Regions with low local velocity magnitude occurred in different parts around the building complex depending on the direction from which the wind was coming and where the wake flow from the buildings was formed. Additionally, funnelling effects between buildings can be observed where the wind was directed around the buildings with increased speed along the passage in between, such as between Buildings A and B in a northerly wind.

Figure 10 shows the plots of local wind velocity magnitude and the UAS drift direction for different incoming wind directions along the paths shown in Figure 9. The UAS drift direction shows the direction in which the UAS would drift in case no flight control input was applied for the UAS such that it would follow where the wind was blowing. For this study, only the wind velocity and the UAS motion in the XY-direction were considered while the Z-direction was ignored for the time being. The UAS drift direction was determined from the angle difference between the direction of the local wind and the UAS flight path. The angle of the local wind direction was computed from the X- and Y-components of the local wind velocity, while the angle of the path was calculated using the X- and Y-coordinates of the UAS flight path. Positive drift direction means the UAS would tend to drift to its left (port) side, and negative means it would tend to drift to its right (starboard) side. If the drift direction is between -90 and 90 degrees, the UAS would be carried forward by the wind, and if it is below -90 or above 90 degrees, the UAS would be pushed back by the wind instead. Signs and

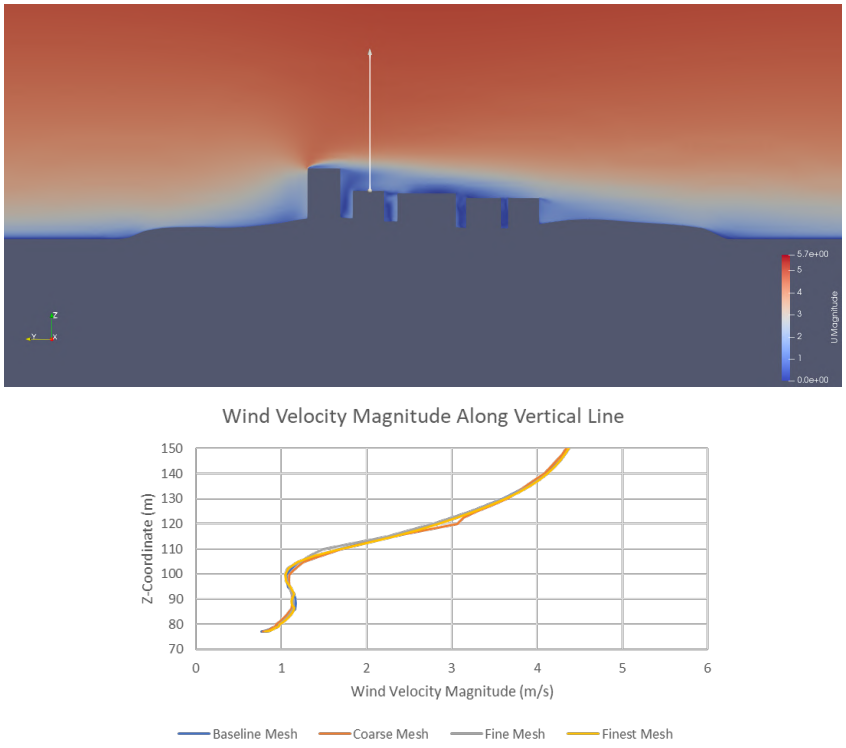

(a) Vertical plane

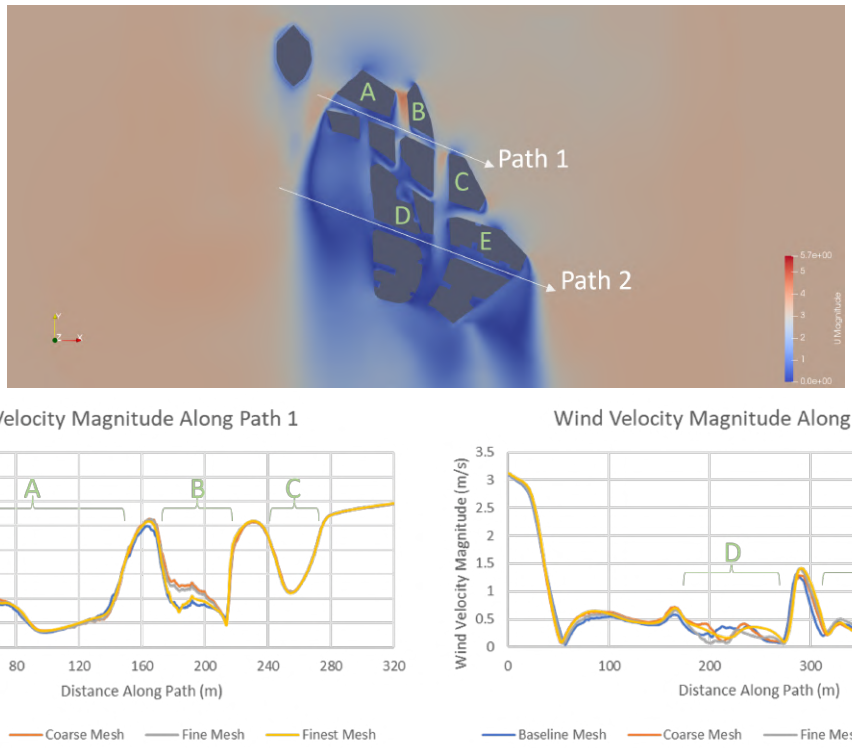

(b) Horizontal plane (Z = 50 m)

Fig. 8 Wind velocity magnitude contours viewed on vertical and horizontal planes, with plots of local wind velocity magnitude for meshes with different levels of refinement along the paths indicated by the arrows.

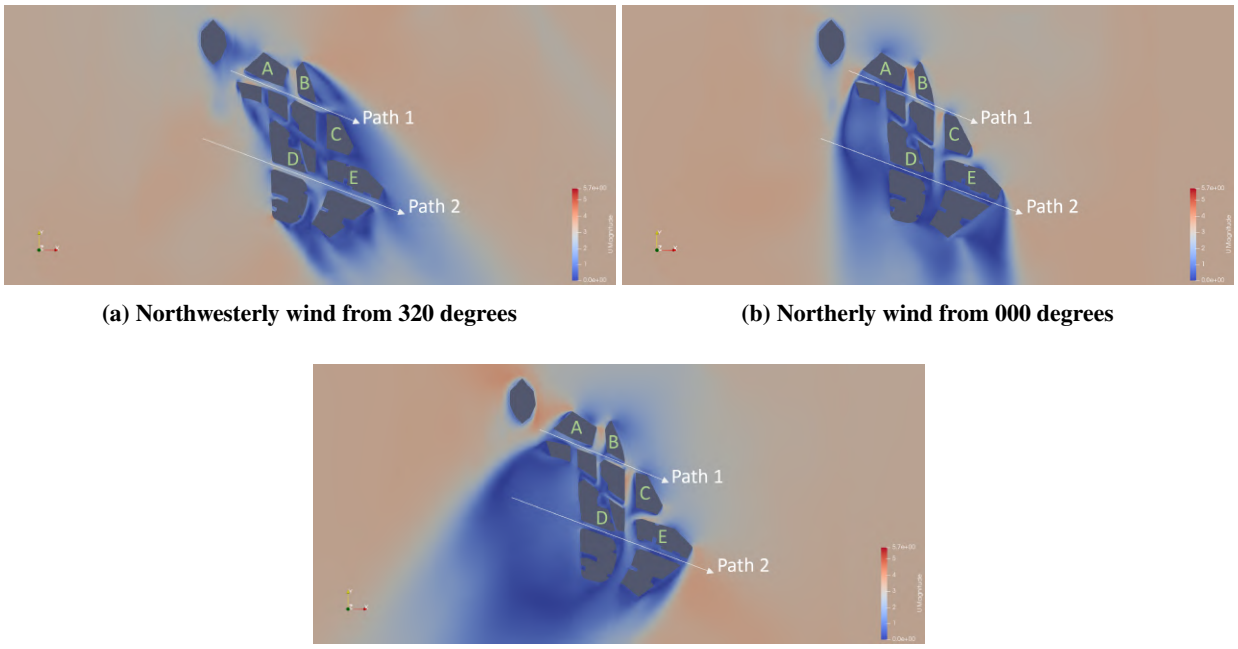

(a) Northwesterly wind from 320 degrees

(b) Northerly wind from 000 degrees

(c) Northeasterly wind from 040 degrees

Fig. 9 Wind velocity magnitude contours on a horizontal plane (Z = 50 meters) from flow simulation using different wind directions, but same reference speed of 2 m/s.

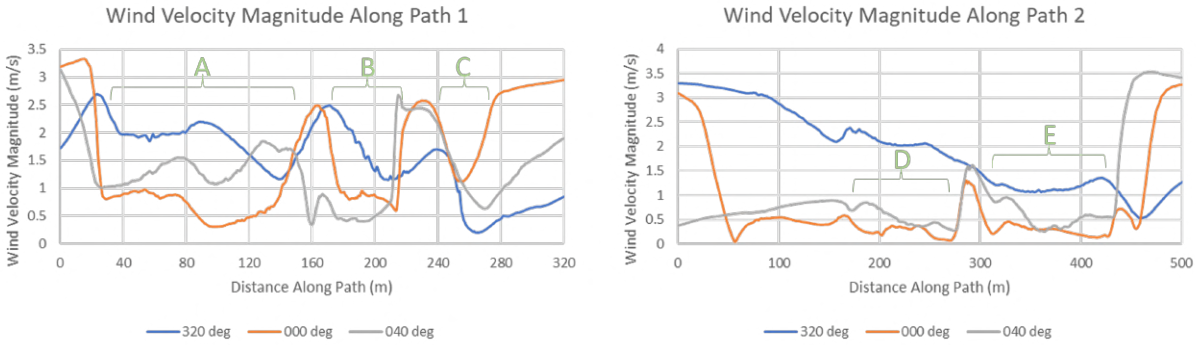

(a) Velocity magnitude, Path 1

(b) Velocity magnitude, Path 2

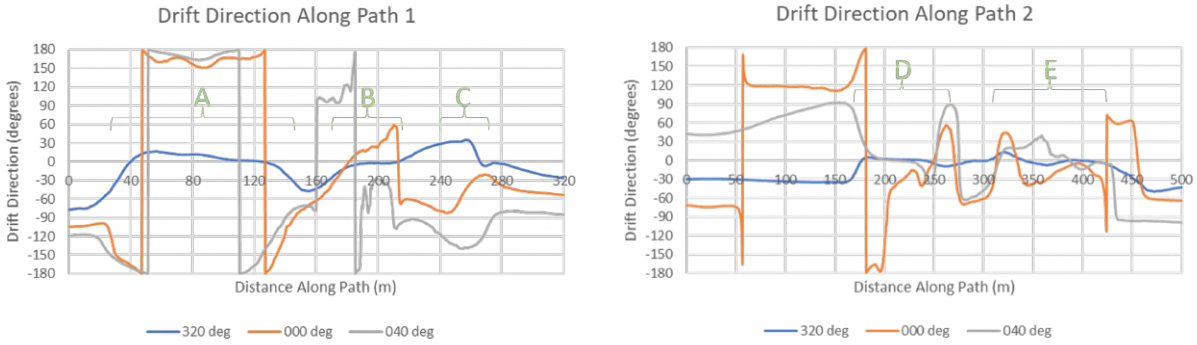

(c) Drift direction, Path 1

(d) Drift direction, Path 2

Fig. 10 Local wind velocity magnitude and UAS drift direction along Path 1 and 2 for different wind directions.

values for the angles of drifting direction in this section follow the conventions of Cartesian quadrants, and they should not be confused or conflated with the angles for the general heading of the incoming wind.

UAS requires flight control inputs to maintain its movement following a designated path. Sudden changes in the local wind velocity experienced by the UAS could cause it to stray from its path, as the UAS might need some time to adjust its control inputs for mitigating effects from the wind. If there is a sudden rise in the local wind speed, the UAS flight control inputs will not have been enough to counter the wind and the UAS will drift in the direction of the local wind. If the local wind speed suddenly drops, the previous inputs for controlling the UAS will become excessive such that they cause the UAS to deviate from its path. The same goes when direction of the local wind changes and the UAS flight control inputs will have to be corrected accordingly. Furthermore, it becomes doubly more important for the UAS to stay within its path when flying through a building complex with narrow passages. Otherwise, the UAS might hit into a building and thus causing UAS failure that may well lead to damages and injuries due to further crashes during its fall.

In Figure 10, the drift direction plot shows where the UAS would tend to drift and the local wind speed plot shows how fast its drift would be, so together they give a sense of how the UAS would be affected by the local wind when flying along a given path. In a northerly wind from 000 degrees and northeasterly wind from 040 degrees, the UAS would be crossing through the wake flow of the buildings along Paths 1 and 2, such that it would see sudden and large changes in the local wind speed and direction. By comparison, the northwesterly wind from 320 degrees was more aligned to Paths 1 and 2 such that the changes in local wind velocity along the paths were more gradual and not as extreme, and there was less sideways drift when flying in between buildings, like on Path 2 passing through Buildings D and E. It can be seen from the plots that every general wind direction creates a particular velocity field within the building complex, such that the UAS flight control inputs will differ for each case to prevent getting drifted by the wind and stay on the path.

C. Velocity Field from Different Inlet Wind Speeds

In this section, the wind velocity field results were obtained from simulation using the same wind direction (coming from 030 degrees), but with different reference speeds from 1 to 4 m/s. Figure 11 shows the wind velocity magnitude contours on a horizontal plane from the simulation cases with different inlet wind reference speeds. The contours are similar in color with one another because the color legend was specific for each case and it covered the full range of the wind speed data obtained for that particular case. Figure 12 shows the plots of normalized local wind velocity magnitude and the UAS drift direction for different incoming wind reference speeds along the paths shown in Figure 11. The wind velocity magnitude of each case was normalized by dividing it with the velocity magnitude at the inlet boundary on the same horizontal plane (i.e. at the same height).

From the plots in Figure 12, the normalized local wind speed appears to be similar between various cases even when using different inlet wind reference speeds, save a few discrepancies such as the regions with low velocity magnitude behind Buildings B, D, and E. The UAS drift direction from the different cases are also in agreement generally, although there may be more uncertainty in the drift direction when the position is between buildings that are more downstream within the wake flow of the building complex, like on Path 2 behind Buildings D and E. Nevertheless, similarity in the results from using different inlet wind reference speeds suggests the possibility of simplifying the simulation of wind field within a building complex, by choosing only one inlet wind reference speed to capture the flow details and obtain data of the wind field, without having to repeat the process with more flow cases for other inlet wind reference speeds.

In addition to analyzing the local wind velocity and the drift direction caused onto the UAS, the contour of Turbulence Kinetic Energy (TKE) could be generated from the flow simulation results to determine the areas within the building complex that should be avoided during UAS flight due to high turbulence kinetic energy. UAS tends to be less stable in maintaining its position and attitude when flying in wind conditions with higher TKE, so a TKE limit can be chosen at the point where the UAS stability would be compromised to unacceptable levels. Figure 13 shows the TKE contours from the flow simulation using wind reference speeds of 2 and 4 m/s. The areas with higher TKE are located around buildings that stand at the most upstream against the wind direction, and these areas increase in size and TKE levels with higher wind speed. The TKE calculated from the wind simulation in this study is lower than the critical TKE value of 6 J/kg assigned by Murray and Anderson in their study [13], and this is due to the lower wind reference speeds that were used in this study such that little to no areas within the building complex reach the critical TKE value.

V. Summary and Future Work

Wind field simulation was carried out to examine the wind velocity field within a building complex and assess the wind effect on UAS flight. Geometry CAD models of the buildings and terrain in the Biopolis complex in Singapore were acquired and incorporated for the wind simulation using steady-state RANS flow solver in OpenFOAM v1912.

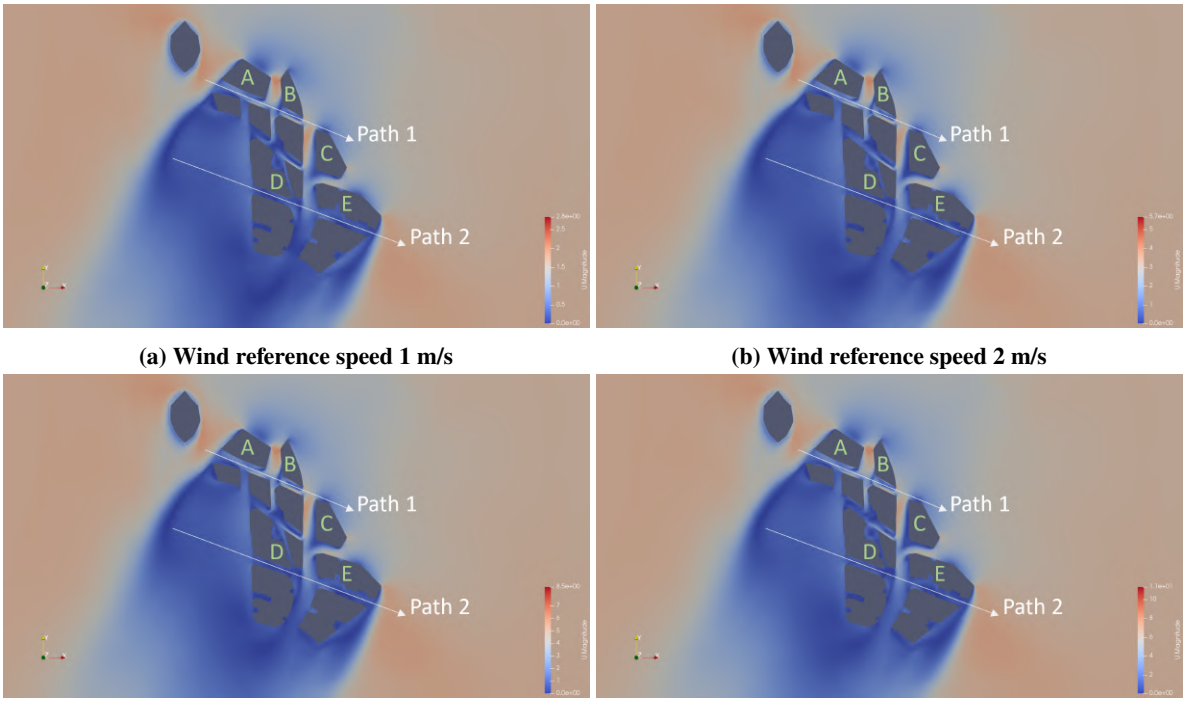

(a) Wind reference speed 1 m/s

(b) Wind reference speed 2 m/s

(c) Wind reference speed 3 m/s

(d) Wind reference speed 4 m/s

Fig. 11 Wind velocity magnitude contours on a horizontal plane (Z = 50 meters) from flow simulation using the same wind direction from 030 degrees, but different reference speeds.

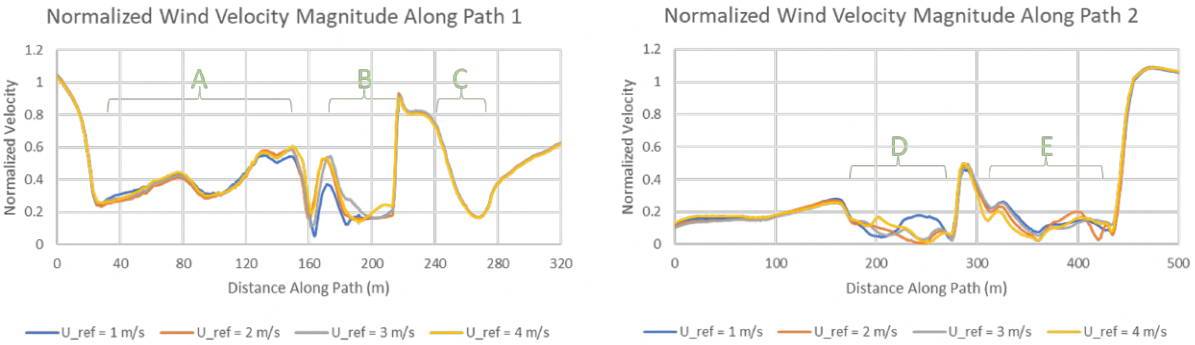

(a) Normalized velocity magnitude, Path 1

(b) Normalized velocity magnitude, Path 2

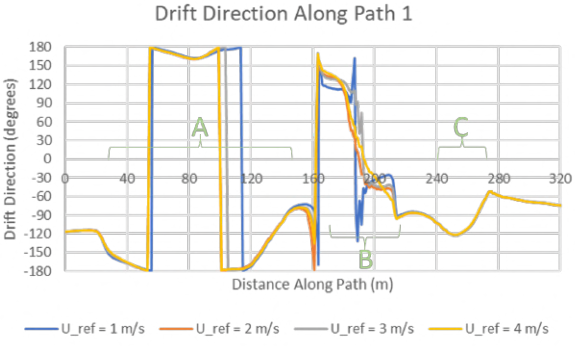

(c) Drift direction, Path 1

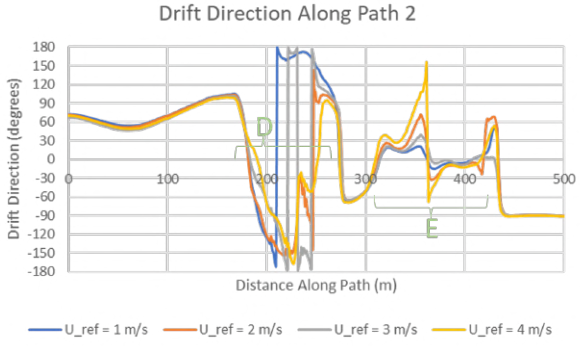

(d) Drift direction, Path 2

Fig. 12 Normalized local wind velocity magnitude and UAS drift direction along Path 1 and 2 for different wind reference speeds.

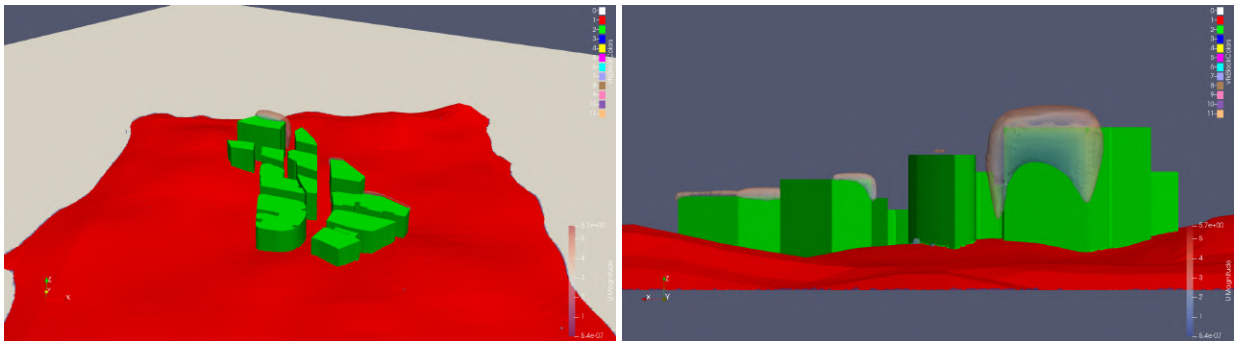

(a) Turbulence kinetic energy 2 J/kg, Wind reference speed 2 m/s

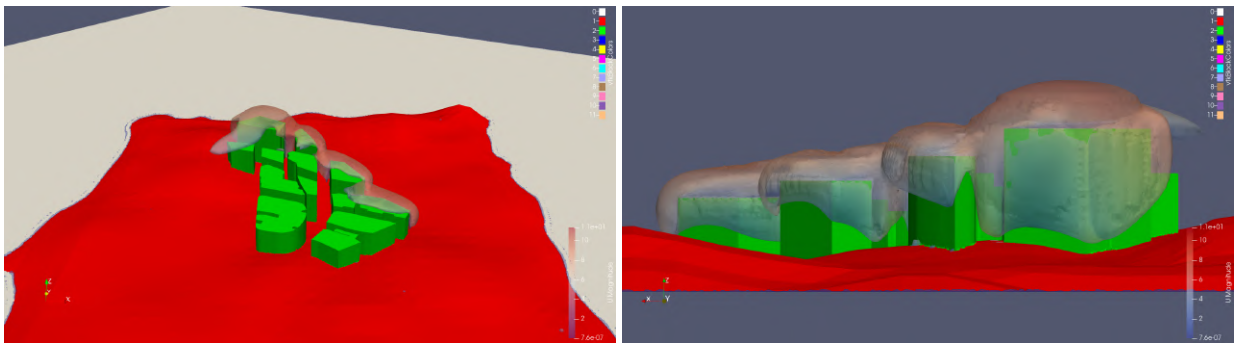

(b) Turbulence kinetic energy 4 J/kg, Wind reference speed 4 m/s

Fig. 13 Top and front views of the turbulence kinetic energy (k) contours from flow simulation using the same wind direction from 030 degrees, but different reference speeds (U_{ref}).

The range of various inlet wind conditions for the simulation was first determined using wind speed and direction readings from a nearby weather station. For each of the various flow cases using different inlet wind reference speeds and directions, the local wind velocity magnitude and direction along different paths were extracted and plotted to examine how the local wind would be affecting the UAS during its flight within the building complex. Additionally, contours of Turbulence Kinetic Energy (TKE) were generated from the results of wind simulation using different wind reference speeds to identify regions within the building complex that have elevated TKE value which could affect the stability of UAS during its flight.

UAS would experience sudden and large changes in the local wind speed and direction when the UAS had to cross through the wake flow of the buildings due to the general wind heading being perpendicular with the flight path. Whereas when the wind was more aligned with the flight path, the change in local wind along the path became more gradual and less extreme. For flow cases with the same inlet wind direction but different reference speeds, similarity in their results was observed when the wind velocity magnitude was normalized, thus suggesting the possibility of simplifying the flow simulation process to study the wind field within a building complex.

For this study, the effect of wind on UAS flight was only examined for flight paths at altitude Z = 50 meters where the UAS would need to navigate through all the buildings in the Biopolis building complex, with only horizontal motion and no vertical component in consideration. At other altitudes, the local wind velocity profile and the hazard that it imposes on UAS flight may be significantly different due to the flow features not present at the current altitude, such as at the top of buildings where recirculation of the wind flow occurs and features different local wind velocity field with more appreciable vertical component. Furthermore, since the wind simulation setup did not include trees, street lights, traffic poles and other detailed features on the ground, the simulation results at very low altitudes close to the ground could not be relied upon for meaningful analysis.

Future work for this study includes experiments to measure the wind velocity in Biopolis and obtain data for validating the simulated wind field. The simulation setup can be improved by using updated geometry models of the buildings and terrain in Biopolis with more details and higher resolution, so that it would reflect more closely to the

real environment. The setup can also be improved to obtain a more accurate wind field, for example by employing Large Eddy Simulation (LES) and time-averaging its results [22], applying more realistic terrain and building boundary conditions to acquire detailed atmospheric flow [23], and coupling the meso-scale and micro-scale weather conditions to obtain more accurate inlet boundary condition for the wind field simulation [24–26]. In addition, instead of only inferring the wind effect from the flow results, the simulated wind data can be utilized for UAS flight simulation using software-in-the-loop (SITL) [27, 28] to study UAS stability and flight behavior when encountering the flow patterns in the urban wind field. Simulation with SITL was previously used to determine the separation requirement between UAS by examining the flight behavior of UAS when encountering the wake vortex from another UAS [29, 30].

Since wind field simulations using CFD are costly in terms of time and computation power, it is unlikely that it can be coupled with the system to manage UAS traffic and operations in real-time. Therefore, efforts have been put into increasing the speed of predicting the wind field of urban spaces. This is achieved by using the results from CFD simulation into other methods, such as for training machine learning algorithms [31, 32], by scaling it according to historical real-time weather readings [33], or by creating a surrogate function which can predict the wind field through inference from the acquired wind measurements at ideal positions [20, 34, 35]. With quicker wind field prediction, warnings can be given ahead of time to prevent UAS from flying into hazardous areas, and flight paths can be planned to achieve the most efficient UAS energy consumption [36–38]. While the findings in this study are still preliminary, this paper along with numerous others highlight the importance of assessing the wind field conditions in urban environments as part of implementing UAS traffic management to ensure the safety of all UAS operations in the future.

Acknowledgements

This research is supported by the National Research Foundation, Singapore, and the Civil Aviation Authority of Singapore, under the Aviation Transformation Programme on Unmanned Aircraft Systems (UAS) in the area of Separation Minima. The support from the Air Traffic Management Research institute (ATMRI) and the School of Mechanical and Aerospace Engineering (MAE), Nanyang Technological University (NTU) is also appreciated. Any opinions, findings, conclusions or recommendations expressed in this material are those of the authors and do not reflect the views of National Research Foundation, Singapore and the Civil Aviation Authority of Singapore. The OpenFOAM flow simulations were made possible by the high performance computing resources allocated by the National Supercomputing Centre (NSCC) Singapore.

References

[1] Chakraborty, S., Dalui, S. K., and Ahuja, A. K., "Wind load on irregular plan shaped tall building - a case study," *Wind and Structures*, Vol. 19, No. 1, 2014, pp. 59–73. https://doi.org/10.12989/was.2014.19.1.059.

[2] Bhattacharyya, B., and Dalui, S. K., "Experimental and Numerical Study of Wind-Pressure Distribution on Irregular-Plan-Shaped Building," *Journal of Structural Engineering*, Vol. 146, No. 7, 2020, pp. 1–14. https://doi.org/10.1061/(ASCE)ST.1943-541X.0002686.

[3] Mou, B., He, B.-J., Zhao, D.-X., and Chau, K.-w., "Numerical simulation of the effects of building dimensional variation on wind pressure distribution," *Engineering Applications of Computational Fluid Mechanics*, Vol. 11, No. 1, 2017, pp. 293–309. https://doi.org/10.1080/19942060.2017.1281845.

[4] van Druenen, T., van Hooff, T., Montazeri, H., and Blocken, B., "CFD evaluation of building geometry modifications to reduce pedestrian-level wind speed," *Building and Environment*, Vol. 163, No. April, 2019, p. 106293. https://doi.org/10.1016/j.buildenv.2019.106293.

[5] Li, M., Qiu, X., Shen, J., Xu, J., Feng, B., He, Y., Shi, G., and Zhu, X., "CFD Simulation of the Wind Field in Jinjiang City Using a Building Data Generalization Method," *Atmosphere*, Vol. 10, No. 6, 2019, p. 326. https://doi.org/10.3390/atmos10060326.

[6] Liu, S., Pan, W., Cheng, X., Zhang, H., Long, Z., and Chen, Q., "CFD Simulations of Wind Flow in an Urban Area with a Full-scale Geometrical Model," *4th International Conference On Building Energy, Environment*, Melbourne, 2018, pp. 174–179.

[7] Liu, S., Pan, W., Zhao, X., Zhang, H., Cheng, X., Long, Z., and Chen, Q., "Influence of surrounding buildings on wind flow around a building predicted by CFD simulations," *Building and Environment*, Vol. 140, No. May, 2018, pp. 1–10. https://doi.org/10.1016/j.buildenv.2018.05.011.

[8] Zheng, S., Wang, Y., (John) Zhai, Z., Xue, Y., and Duanmu, L., "Characteristics of wind flow around a target building with different surrounding building layers predicted by CFD simulation," *Building and Environment*, Vol. 201, No. March, 2021, p. 107962. https://doi.org/10.1016/j.buildenv.2021.107962.

[9] Wise, D., Boppana, V., Li, K., and Poh, H., "Effects of minor changes in the mean inlet wind direction on urban flow simulations," *Sustainable Cities and Society*, Vol. 37, No. November 2017, 2018, pp. 492–500. https://doi.org/10.1016/j.scs.2017.11.041.

[10] Sutherland, M., Etele, J., and Fusina, G., "Urban Wake-Field Generation Using Large-Eddy Simulation for Application to Quadrotor Flight," *Journal of Aircraft*, Vol. 53, No. 5, 2016, pp. 1224–1236. https://doi.org/10.2514/1.C033624.

[11] Mohamed, A., Carrese, R., Fletcher, D., and Watkins, S., "Scale-resolving simulation to predict the updraught regions over buildings for MAV orographic lift soaring," *Journal of Wind Engineering and Industrial Aerodynamics*, Vol. 140, 2015, pp. 34–48. https://doi.org/10.1016/j.jweia.2015.01.016.

[12] Watkins, S., Mohamed, A., and Ol, M. V., "Gusts Encountered by MAVs in Close Proximity to Buildings," *AIAA Scitech 2019 Forum*, American Institute of Aeronautics and Astronautics, Reston, Virginia, 2019, pp. 1–9. https://doi.org/10.2514/6.2019-0900.

[13] Murray, C. W., and Anderson, D., "A CFD-based procedure for airspace integration of small unmanned aircraft within congested areas," *International Journal of Micro Air Vehicles*, Vol. 9, No. 4, 2017, pp. 235–252. https://doi.org/10.1177/1756829316669957.

[14] "Realtime Weather Readings across Singapore," , 2016. URL https://data.gov.sg/dataset/realtime-weather-readings.

[15] "Singapore Open Data Licence version 1.0," , 2016. URL https://data.gov.sg/open-data-licence.

[16] Meteorological Service Singapore, "ANNUAL CLIMATOLOGICAL REPORT 2018," , 2019. URL http://www.weather.gov.sg/wp-content/uploads/2019/03/Annual-Climatological-Report-2018.pdf.

[17] Meteorological Service Singapore, "Climate of Singapore," , Accessed on May 3, 2023. URL http://www.weather.gov.sg/climate-climate-of-singapore/.

[18] Mughal, M. O., Li, X., Yin, T., Martilli, A., Brousse, O., Dissegna, M. A., and Norford, L. K., "High-Resolution, Multilayer Modeling of Singapore's Urban Climate Incorporating Local Climate Zones," *Journal of Geophysical Research: Atmospheres*, Vol. 124, No. 14, 2019, pp. 7764–7785. https://doi.org/10.1029/2018JD029796, URL https://onlinelibrary.wiley.com/doi/abs/10.1029/2018JD029796.

[19] Earth Resources Observation and Science (EROS) Center, "USGS EROS Archive - Digital Elevation - Shuttle Radar Topography Mission (SRTM) 1 Arc-Second Global," , 2018. URL https://www.usgs.gov/centers/eros/science/usgs-eros-archive-digital-elevation-shuttle-radar-topography-mission-srtm-1.

[20] Sousa, J., García-Sánchez, C., and Gorlé, C., "Improving urban flow predictions through data assimilation," *Building and Environment*, Vol. 132, No. November 2017, 2018, pp. 282–290. https://doi.org/10.1016/j.buildenv.2018.01.032.

[21] Blocken, B., Carmeliet, J., and Stathopoulos, T., "CFD evaluation of wind speed conditions in passages between parallel buildings—effect of wall-function roughness modifications for the atmospheric boundary layer flow," *Journal of Wind Engineering and Industrial Aerodynamics*, Vol. 95, No. 9-11, 2007, pp. 941–962. https://doi.org/10.1016/j.jweia.2007.01.013.

[22] Robinson, M., Klimenko, V., Diao, Q., Bieringer, P., and Annunzio, A., "Validation of Simulated Urban Microscale Weather Pertinent to Aviation Interests," *AIAA AVIATION 2020 FORUM*, Vol. 1 PartF, American Institute of Aeronautics and Astronautics, Reston, Virginia, 2020, pp. 1–34. https://doi.org/10.2514/6.2020-2866.

[23] Giersch, S., El Guernaoui, O., Raasch, S., Sauer, M., and Palomar, M., "Atmospheric flow simulation strategies to assess turbulent wind conditions for safe drone operations in urban environments," *Journal of Wind Engineering and Industrial Aerodynamics*, Vol. 229, No. August, 2022, p. 105136. https://doi.org/10.1016/j.jweia.2022.105136.

[24] Tabib, M. V., Midtbø, K. H., Skaslien, T., Rasheed, A., and Kvamsdal, T., "TOWARDS UNDERSTANDING WIND IMPACT FOR DRONE OPERATIONS: A COMPARISON OF WIND MODELS OPERATING ON DIFFERENT SCALES IN A NESTED MULTISCALE SET-UP," *14th International Conference on CFD in Oil & Gas, Metallurgical and Process Industries*, SINTEF Academic Press, Trondheim, NORWAY, 2020.

[25] Tabib, M. V., Midtbø, K. H., Rasheed, A., Kvamsdal, T., and Skaslien, T., "A nested multi-scale model for assessing urban wind conditions : Comparison of Large Eddy Simulation versus RANS turbulence models when operating at the finest scale of the nesting." *Journal of Physics: Conference Series*, Vol. 2018, No. 1, 2021, p. 012039. https://doi.org/10.1088/1742-6596/2018/1/012039.

[26] Bouris, D., Triantafyllou, A. G., Krestou, A., Leivaditou, E., Skordas, J., Konstantinidis, E., Kopanidis, A., and Wang, Q., "Urban-Scale Computational Fluid Dynamics Simulations with Boundary Conditions from Similarity Theory and a Mesoscale Model," *Energies*, Vol. 14, No. 18, 2021, p. 5624. https://doi.org/10.3390/en14185624.

[27] Wang, C. H. J., Nathanael, J. C., Ng, E. M., Ng, B. F., and Low, K. H., "Framework for the Estimation of Safe Wake Separation Distance between Same-Track Multi-Rotor UAS," *AIAA Scitech 2021 Forum*, American Institute of Aeronautics and Astronautics, Reston, Virginia, 2021, pp. 1–14. https://doi.org/10.2514/6.2021-0708.

[28] Wang, C. J., and Low, K. H., "Software-in-the-loop investigation of wake-vortex-encounter-response of identical multirotor pair with PX4 attitude controller," *Aerospace Science and Technology*, Vol. 117, 2021, p. 106967. https://doi.org/10.1016/j.ast.2021.106967.

[29] Nathanael, J. C., Wang, C. H. J., and Low, K. H., "A Study on Circulation Strength Decay Over Time of Quadrotor Wake Using Large Eddy Simulation," *AIAA SCITECH 2022 Forum*, American Institute of Aeronautics and Astronautics, Reston, Virginia, 2022, pp. 1–12. https://doi.org/10.2514/6.2022-0155.

[30] Wang, C. H. J., Nathanael, J. C., and Low, K. H., "Comparison of Small Multirotor Wake Vortex of Different Weight Class and Rotor Configurations via Numerical Simulation," *AIAA SCITECH 2023 Forum*, American Institute of Aeronautics and Astronautics, Reston, Virginia, 2023, pp. 1–8. https://doi.org/10.2514/6.2023-1012.

[31] Vuppala, R. K. S. S., and Kara, K., "A Novel Approach in Realistic Wind Data Generation for The Safe Operation of Small Unmanned Aerial Systems in Urban Environment," *AIAA AVIATION 2021 FORUM*, American Institute of Aeronautics and Astronautics, Reston, Virginia, 2021, pp. 1–10. https://doi.org/10.2514/6.2021-2505.

[32] Vuppala, R. K. S. S., and Kara, K., "Wind Field Prediction in Urban Spaces for small Unmanned Aerial Systems using Convolutional Autoencoders," *AIAA AVIATION 2022 Forum*, American Institute of Aeronautics and Astronautics, Reston, Virginia, 2022, pp. 1–13. https://doi.org/10.2514/6.2022-3605.

[33] Gianfelice, M., Aboshosha, H., and Ghazal, T., "Real-time Wind Predictions for Safe Drone Flights in Toronto," *Results in Engineering*, Vol. 15, No. June, 2022, p. 100534. https://doi.org/10.1016/j.rineng.2022.100534.

[34] Sousa, J., and Gorlé, C., "Computational urban flow predictions with Bayesian inference: Validation with field data," *Building and Environment*, Vol. 154, No. February, 2019, pp. 13–22. https://doi.org/10.1016/j.buildenv.2019.02.028.

[35] Patrikar, J., Moon, B. G., and Scherer, S., "Wind and the City: Utilizing UAV-Based In-Situ Measurements for Estimating Urban Wind Fields," *2020 IEEE/RSJ International Conference on Intelligent Robots and Systems (IROS)*, IEEE, 2020, pp. 1254–1260. https://doi.org/10.1109/IROS45743.2020.9340812.

[36] Hong, D., Lee, S., Cho, Y. H., Baek, D., Kim, J., and Chang, N., "Least-Energy Path Planning With Building Accurate Power Consumption Model of Rotary Unmanned Aerial Vehicle," *IEEE Transactions on Vehicular Technology*, Vol. 69, No. 12, 2020, pp. 14803–14817. https://doi.org/10.1109/TVT.2020.3040537.

[37] Baskar, D., and Gorodetsky, A., "A Simulated Wind-field Dataset for Testing Energy Efficient Path-Planning Algorithms for UAVs in Urban Environment," *AIAA AVIATION 2020 FORUM*, Vol. 1 PartF, American Institute of Aeronautics and Astronautics, Reston, Virginia, 2020, pp. 1–11. https://doi.org/10.2514/6.2020-2920.

[38] Palazzetti, L., "Routing Drones Being Aware of Wind Conditions: a Case Study," *2021 17th International Conference on Distributed Computing in Sensor Systems (DCOSS)*, IEEE, 2021, pp. 343–350. https://doi.org/10.1109/DCOSS52077.2021.00062.